Rapid Evaluation of Dynamic Electronic Disorder in Molecular Semiconductors

Alessandro Landi [a,b] and Alessandro Troisi [*,a]

[a] *Department of Chemistry, University of Liverpool, Liverpool L69 3BX, United Kingdom*
[b] *Dipartimento di Chimica e Biologia Adolfo Zambelli, Università di Salerno, Via Giovanni Paolo II, I-84084 Fisciano (SA), Italy*
* A.Troisi@liverpool.ac.uk

Abstract

One of the key factors limiting the charge mobility of molecular semiconductors is the fluctuation of transfer integrals, also known as dynamic disorder. This is a manifestation of the non-local electron phonon coupling, a property that is computationally expensive to evaluate and, so far, prevented the study of this property on large datasets of molecules. In this paper we describe a methodology for the fast evaluation of the dynamic electronic disorder for molecular semiconductors from their crystalline structure. The computation is accelerated by (i) the evaluation of the Cartesian gradient of transfer integral and (ii) the use of approximate phonons evaluated within the rigid body approximation. The quality of the approximations is checked against less approximated alternatives. The method is used to study a range of molecular crystals and some general trends on the behaviour of the non-local electron-phonon coupling are discussed. A strategy to find the optimal relative position between interacting molecules is proposed.

Introduction

A number of highly desirable properties motivates the research into organic semiconductors: they can be processed at lower temperatures than inorganic semiconductors, they have good mechanical properties like high flexibility and strength and their chemical/physical properties can be easily tuned by using different functional groups.[1–3] These materials are currently used in devices like organic field-effect transistors (OFET),[3,4] organic light emitting diodes (OLED),[5] and organic solar cells (OSC).[6] The charge mobility of organic semiconductors is their main electronic characteristic and the materials developed within the past few years, with mobilities exceeding 1 $cm^2V^{-1}s^{-1}$, can now compete with that of amorphous silicon.[7] Despite the intense research effort all new organic semiconductors have usually been discovered by trial and error and, even retrospectively, it was not always possible to explain why some materials were better than others. Many authors are advocating the use of computer-aided materials discovery[8] to accelerate the pace of organic semiconductor discovery.[3,8–10] A major bottleneck in the case of molecular crystals is the great challenge of performing crystal structure prediction on large sets of hypothetical molecules[11,12] and the observation that the intermolecular arrangement rather than the isolated molecular properties is the key determinant of the mobility[2]. The best contribution that computational methods could give at the moment is the prediction of the mobility from the crystalline structure of the semiconductor. A tool able to perform such prediction would be highly beneficial considering that substantial experimental effort is required to grow ultra-pure single-crystalline samples for OFET measurements, while the crystalline structures of the material are typically known shortly after the initial synthesis.

The computational methodology for predicting the charge mobility must be related to a mechanism of charge transport as different mechanisms require the evaluation of different parameters. For example, if one wishes to use a charge hopping approach within Marcus theory, the mobility can be predicted from the transfer integral between nearest neighbour molecules and the reorganization energy of the isolated molecule,[13–15] an approach that can be easily implemented to screen thousands of molecules.[16] Unfortunately, there are serious limitation with describing charge transport via a hopping approach,[17] and the large reported mobility with the evidence

of Hall effects[18,19] suggests that the charge propagates coherently. A family of alternative models have emerged based on the observation that the transfer integral undergoes large fluctuations because of thermal motions.[20–23] This effect, known as dynamic disorder, is due to the strong modulation of the transfer integral by low frequency molecular phonons, i.e. it is a manifestation of the non-local electron-phonon coupling. A number of numerical methods have been proposed to compute the mobility for such systems including Ehrenfest dynamics[24], modified surface hopping[25,26], open quantum systems dynamics,[27,28] many-body physics methods[29] on model Hamiltonians[30] or realistic chemical models.[31–35] Fratini et al. proposed a method that is particularly appealing to the intuition based on the evaluation of a *transient localization*.[36,37] When applied to a family of realistic semiconductors it demonstrated excellent predictive power and was used to build a map of molecular semiconductors that are less susceptible to disorder.[21] It is therefore evident that, regardless of the detailed description of transport, the evaluation of the non-local-electron phonon coupling has become an essential component for the analysis of existing materials or the discovery of new ones. All these models predict that the mobility increases if the dynamic disorder decreases but, up to now, there are no design principles for molecules or materials displaying the smallest possible amount of nonlocal electron-phonon coupling. The analysis of the nonlocal electron-phonon coupling for a great number of materials can reveal interesting chemical patterns and, possibly, suggest new chemical design rules for materials insensitive to disorder.

The evaluation of the non-local electron-phonon coupling for molecular crystals has been performed several times,[38,39] but the available methods are not suitable to explore a large data set of materials. The most expensive component of the calculation is the evaluation of the crystal vibrations and, for this reason, many have adopted empirical force fields.[40,41] These can be inaccurate (they have not been parametrized to reproduce low frequency vibration) and, more importantly, cannot describe (without re-parametrization) the novel chemical functionalities introduced in many new compounds. First principle evaluations of the phonons of molecular crystals, albeit fairly well established[42–45] are very rarely performed on materials with hundreds of atoms in the unit cell – a common occurrence in organic semiconductors – and are certainly not suitable as a routine protocol for exploring new materials.

The aim of this paper is to present a methodology for the evaluation of the dynamic electronic disorder in organic materials in a significantly reduced computational time relying on two main ideas: (i) the evaluation of the electron-phonon coupling with respect to cartesian displacement and (ii) the use of simplified phonons evaluated in the framework of the rigid-body approximation,[2,46] where each molecule is assumed to oscillate independently, with the great advantage of separating effectively the internal (intramolecular vibrations) and external (intermolecular vibrations) degrees of freedom. Here we test our methodology on some molecules widely studied in the literature, comparing a selection of our results with data obtained with more accurate approaches, e.g. taking into account the hybridization of intra- and inter- molecular vibration modes.[47,48]

Methods

Definitions. We use a tight-binding Hamiltonian for the description of the charge transport in organic semiconductor, which can be written as a sum of 3 contributions: the electronic part, the phonon part and their interaction

$$H = H^{el} + H^{ph} + H^{el-ph}. \tag{1}$$

The electronic Hamiltonian can be written as

$$H^{el} = \sum_i \epsilon_i |i\rangle\langle i| + \sum_{i,j\neq i} J_{ij} |i\rangle\langle j|, \tag{2}$$

where the basis set $|i\rangle$ contains one-electron states localized on site *i* (only one state per site is considered, e.g. the molecular HOMO for hole transport), ϵ_i is the site electronic energy, J_{ij} is the transfer integral and the summation is limited to the nearest neighbours pair. The phonon term is described by:

$$H^{ph} = \sum_M \hbar\omega_M \left(-\frac{1}{2}\frac{\partial^2}{\partial Q_M{}^2} + \frac{1}{2} Q_M{}^2 \right), \tag{3}$$

where the index M runs over all nuclear modes with frequency ω_M and Q_M is the dimensionless coordinate of the normal mode. The electron-phonon coupling part of the Hamiltonian is

$$H^{el-ph} = \sum_i \sum_M g_{i,M} Q_M \left|i\right\rangle\left\langle i\right| + \sum_{i,j\neq i} \sum_M g_{ij,M} Q_M \left|i\right\rangle\left\langle j\right|, \tag{4}$$

where the total electron-phonon coupling is explicitly separated in terms of the local ($g_{i,M}$) and the nonlocal ($g_{ij,M}$) electron-phonon couplings. The former concerns the modulation of the site energies, while the latter describes the modulation of the transfer integrals. A number of work have described the calculation of the local electron-phonon coupling,[43] which is now routinely achievable. This work will only consider the evaluation of the non-local electron-phonon coupling $g_{ij,M}$, which is ultimately responsible of the dynamic disorder and the fluctuation of the transfer integral. The latter can be computed at a given temperature from the electron-phonon coupling terms as:[46]

$$\sigma_{ij}{}^2 = \left\langle \left(J_{ij} - \left\langle J_{ij} \right\rangle \right)^2 \right\rangle = \sum_M \frac{\left|g_{ij,M}\right|^2}{2} \coth\left(\frac{\hbar\omega_M}{2k_B T} \right), \tag{5}$$

where $k_B T$ is the thermal energy. An efficient evaluation of eq. (5) is the goal of the reminder of this section.

Computation of non-local electron-phonon coupling. The transfer integrals J_{ij} depend on the set of displacements $\{Q_M\}$. The couplings $\{g_{ij,M}\}$ appear in the second term of the Taylor series of the expansion of J_{ij} around the equilibrium position:

$$J_{ij}(\{Q_M\}) \cong J_{ij}(\{Q_M\} = 0) + \sum_M g_{ij,M} Q_M + \sum_{M,N} \frac{\partial^2 J_{ij}}{\partial Q_M \partial Q_N} Q_M Q_N + \ldots \tag{6}$$

i.e. the $\{g_{ij,M}\}$ can be evaluated as

$$g_{ij,M} = \left. \frac{\partial J_{ij}(\{Q_M\})}{\partial Q_M} \right|_{\{Q_M\}=0} \tag{7}$$

The transfer integrals in this work have been evaluated as:[49]

$$J_{ij}(\{Q_M\}) = \left\langle \phi_i^0(\{Q_M\}) \middle| F(\{Q_M\}) \middle| \phi_j^0(\{Q_M\}) \right\rangle, \tag{8}$$

where ϕ_i^0 and ϕ_j^0 are the localised highest-occupied molecular orbitals (HOMO) of molecule i and j, respectively, and F is the Fock operator of the dimer system. The suffix *0* indicates that the orbitals are unperturbed, i.e. computed for the isolated molecule. It is alternatively possible to evaluate the same matrix elements using the Fock matrix built using the density matrix of the non-interacting monomer. Our test with pentacene, rubrene and tetracene indicate only small differences (under 5% with correlation coefficient between the two calculations r^2=0.995). We have performed additional tests using the methodology proposed in ref. 50 and based on transforming the Fock matrix extracted from adiabatic first-principle calculations, also obtaining equally consistent results.

The sign of the transfer integral depends on an arbitrary phase of the orbital but the signs of all transfer integral of a solid need to be evaluated consistently, e.g. once a phase is chosen for an orbital all transfer integral must be reported with that phase. Electronic properties like band structure or charge mobility are incorrect if one does not keep track of the relative transfer integral sign. In this work we select the phase arbitrarily, making the phase identical for orbitals on translationally invariant molecules and we report one of the correct sign combinations (the other can be derived trivially from eq. (8)).

We represent the mode M as a vector of Cartesian displacements $Q_M = \{x_k^M\}$, which spans the entire supercell, writing the electron-phonon coupling as:

$$g_{ij,M} = \nabla J_{ij} \cdot Q_M \,, \tag{9}$$

where ∇J_{ij} is the Cartesian gradient of the transfer integral, i.e. the derivative of the transfer integral with respect to the Cartesian displacement of an atom k:

$$\nabla J_{ij} = \left\{ \frac{\partial J_{ij}}{\partial x_k} \right\}. \tag{10}$$

Here the elements of this vector are zero if displacements x_k do not belong to molecule i or j.

The formulation in eq. (9) is useful because the first term of the product only includes $6N_A$ differentiations (N_A being the number of atoms in one molecule) and the second term does not depend on the transfer integral. Besides, it should be noted that, while the gradient of the transfer integral can be evaluated relatively quickly (e.g. in less than 1 day per typical molecule using 16 processors), the computation of all the lattice phonons is a time-consuming task, especially if a good sampling of the Brillouin zone is required.[38,46,48]

Approximate phonons. We significantly speed up the computations by using simplified phonons evaluated assuming that each molecule oscillates independently from the others (Einstein dispersionless phonons), with a strict separation between intramolecular and intermolecular degrees of freedom. The intramolecular vibrational modes are assumed to be equal to the vibrations of the isolated molecule. This is an excellent approximation at least for the high frequency modes, which display only moderate frequency variations between solution and solid-state phases.[51,52]

To describe the intermolecular motion, we consider the rigid motion of each molecule surrounded by the neighbouring molecules frozen in their equilibrium position. The quality of such approximation, not known a priori but used for example in ref. [53–55], will be evaluated in the next section in the context of determining the dynamic disorder of specific materials. In practice, we define six rigid displacement modes $q_1 \ldots q_6$ (three translations and three rotations in reduced mass coordinates) and evaluate numerically the 6×6 Hessian matrix $P_{ij} = \partial^2 E / \partial q_i \partial q_j$, where E is the total energy of a cluster containing a molecule surrounded by all molecules in van der Waals contact. The eigenvalues ω_M^2 of the Hessian give the square of the frequencies of the rigid molecule modes and the corresponding eigenvectors $w_{j,M}$ provide a representation of the rigid molecules modes Q_M as linear combination of the original roto-translational modes:

$$Q_M = \sum_{j=1}^{6} w_{j,M} q_j \tag{11}$$

Computational Details

The level of the computation was selected to be consistent with the reminder of the approximations and the intention to perform calculations on a large set of molecules. The validation of the methodology against less approximated alternatives is given in the result section. Electronic structure and normal modes have been calculated by employing the self-consistent-charge density-functional tight-binding (SCC-DFTB) method as implemented in the DFTB+ software package.[56,57] The DFTB method is a non-orthogonal tight-binding method based on a second-order expansion of the DFT total energy expression. Thanks to a series of approximations, including the two-centre approximation and the use of minimal atomic basis sets, the elements of Hamiltonian and overlap matrices are evaluated starting from pre-computed values, so computations are about 3-4 orders of magnitudes faster using DFTB rather than DFT.[57,58] Optimized structures have been obtained using the conjugate gradient method with a force-threshold criterion of 10^{-8} Hartree per Bohr radius, while holding fixed the experimental crystalline lattice constants. We have used periodic boundary conditions (PBC) employing a

4×4×4 Monkhorst-Pack *k*-point sampling scheme.[59] The DFTB-D3 formalism[60] is used to take into account the van der Waals interaction in the crystalline phase.

Calculations of the transfer integrals are carried out at the B3LYP/3-21g* level of theory as implemented in Gaussian 16.[61] Selected calculations have been performed also using different functionals and basis set (B3LYP/3-21g*, B3LYP/6-31g*, B3LYP/6-311g**, PBE/6-31g*) as discussed in the result section. ∇J_{ij} has been evaluated by using the finite-difference 2-point approximation, using displacement of ±0.01 Å.

It should be noted that it is not convenient to use DFTB for the transfer integral as the method is known to severely underestimate this quantity because of the minimal basis set used.[62–66] The proposed solution to this problem, a case-by-case recalibration of additional diffuse basis set in DFTB,[62,63] would not be convenient for the study of a large range of materials.

To construct the Hessian matrix P_{ij}, the second derivative of the energy has been evaluated numerically by performing single-point DFTB+ calculation on a supercell in which the molecule of interest is distorted along the rigid molecular displacements, in the presence of periodic boundary conditions (PBC). The supercell size is chosen so that in presence of PBC the molecule of interest is not in van der Waals contact with its repetition.

Results

Systems studied

We have studied 12 crystalline semiconductors, shown in Fig. 1 with their full chemical name in the caption, including oligoacenes, oligothienoacenes, tetrathiafulvalenes and derivatives. These systems are widely studied in the literature[7,13,21,67] as they show the highest mobilities recorded up to now.

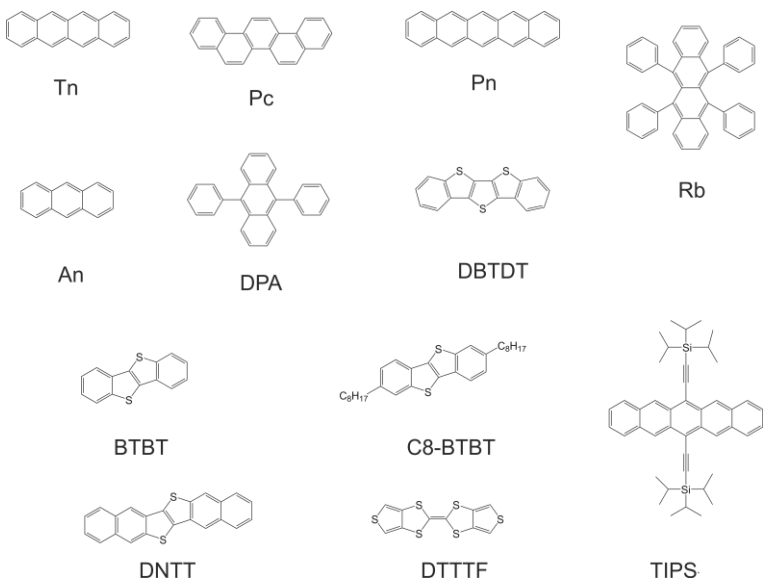

Figure 1. The organic molecules studied in this work. Full names are: An=anthracene; Pn = pentacene; Rb = rubrene; Tn = tetracene; Pc = picene; BTBT = [1]benzothieno[3,2-b][1]benzothiophene; C8-BTBT = 2,7-Dioctyl[1]benzothieno[3,2-b][1]benzothiophene; TIPS = 6,13-Bis(triisopropylsilylethynyl)pentacene; DPA = Diphenil-anthracene; DTTTF = Dithieno-tetratiofulvalene; DBTDT = Dibenzo-thieno-dithiophene; DNTT = Dinaphtho-thieno-thiophene.

As shown elsewhere,[68–71] the majority of molecular semiconductors have a crystal structure with a high-mobility plane, while the mobility perpendicular to this plane is 1-2 orders of magnitude smaller. Here we focus on the high-mobility plane, and, for convenience in reporting our results, we refer to a standard 2D lattice where there can be up to three nearest-neighbour transfer integrals (Fig. 2). Indeed, allowing for some of the transfer integrals to be zero, or for pairs of parameters to be identical, such a lattice can describe the vast majority of high-mobility organic molecular semiconductors.[21]

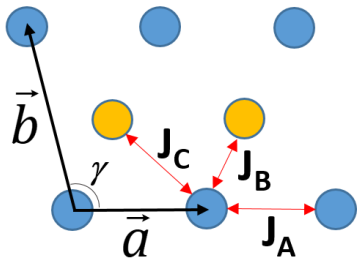

Figure 2. Definition of a standard 2D lattice used to present the parameters needed for the calculation of the mobility. *a* and *b* identify any two crystallographic axes and γ is the angle between them.

Using this layout, we report in Table 1 the transfer integral (J), the norm of the transfer integral gradient ($|\nabla J|$) and the fluctuation of the transfer integral (σ) evaluated at T=300 K for each pair in the high-mobility plane of the molecules in Fig. 1. In particular the crystal structure is derived from the Cambridge Structural Database (CSD)[72] and the molecule pair is identified by: (i) the ID of the first molecule of the pair in the reference cell (ID is a number varying between 1 and the number of the independent molecules in the unit cell), (ii) the ID of the other molecule constituting the pair, (iii) three integers n_1, n_2, n_3 defining the translation $n_1\vec{v}_1 + n_2\vec{v}_2 + n_3\vec{v}_3$ of the second molecule with respect to the first one ($\vec{v}_1, \vec{v}_2, \vec{v}_3$ are the lattice vectors in the reference crystallographic structure).

Table 1. List of pairs in the high-mobility plane for molecules in Fig. 1 and relative values for: the transfer integral (J), the norm of the transfer integral gradient ($|\nabla J|$) and the fluctuation of the transfer integral (σ) at 300 K. For each molecule the CSD (from which all the CIF files have been obtained) code is provided. The molecules constituting each pair are labeled according to Fig. 2 and further identified as explained in the main text. All values are obtained using B3LYP/3-21g*.

Molecule & CSD code	Label	ID_1, ID_2, n_1, n_2, n_3	J (meV)	$\|\nabla J\|$ (mev/Å)	σ (meV)	σ (meV) other works
An (599019)	A	1, 1, 0, -1, 0	−61.2	176	14.6	10-11 [a]
	B	1, 2, -1, -1, -1	+35.1	724	41.4	20-21 [a]
Tn (IUCr A03426)	A	1, 1, 0, −1, 0	+5.60	180	17.2	14-16 [a]
	B	1, 2, 0, 0, 0	+18.9	375	22.8	19-21 [a]
	C	1, 2, −1, 0, 0	−86.4	301	21.4	17-18 [a]
Pn (665900)	A	1, 1, −1, 0, 0	−74.9	142	13.1	14-15 [b]
	B	1, 2, 0, 0, 0	−102	218	23.9	24-28 [b]
	C	1, 2, −1, 0, 0	−96.9	249	22.7	22-24 [b]
Rb (605647)	A	1, 1, −1, 0, 0	+140	289	46.3	49.1 [c] - 51 [d]
	B	1, 2, 0, 0, 0	−21.3	124	18.7	9.7[c] - 9.9 [d]
Pc (560122)	A	1, 1, 0, −1, 0	+115	217	17.9	
	B	1, 2, 0, 0, 0	−89.8	527	24.1	
	C	1, 2, 1, −1, 0	−81.8	526	27.8	
BTBT (975935)	A	1, 1, 0, −1, 0	+119	1222	46.7	
	B	1, 2, 0, 0, 0	−23.4	808	43.2	
DTTTF (1236389)	A	1, 1, 0, −1, 0	+114	1134	84.2	
	B	1, 2, −1, −1, 0	−55.0	537	87.5	
DNTT (644240)	A	1, 1, −1, 0, 0	+131	197	15.2	
	B	1, 2, −1, 0, 1	−146	712	53.7	
DBTDT (1236389)	A	1, 1, 0, 0, -1	+15.5	124	9.47	
	B	1, 3, -1, 0, 1	−20.8	208	12.6	
	C	1, 3, 0, 0, 0	−68.1	245	14.4	
DPA (113041)	B	1, 3, -1, 0, 0	36.891	190	11.5	
	C	1, 2, 0, 0, 0	-44.852	199	13.3	
TIPS (172476)	A	1, 1, 0, −1, 0	+3.01	33.1	12.3	
	B	1, 1, −1, 1, 0	+45.3	762	101	
	C	1, 1, −1, 0, 0	+45.3	1147	144	
	A	1, 1, −1, 0, 0	+70.2	1464	148	

C8-BTBT (679293)	B C	1, 2, −1, −1, 0 1, 2, 0, 0, 0	+70.2 −9.65	1616 448	306 71.2	

Reference values from: [a] ref. [38]; [b] ref. [43]; [c] ref. [48]; [d] ref. [73];

Validation of the approach

Before discussing the results in Table 1, we report the outcomes of tests concerning (i) the sensitivity of the transfer integral to the density functional and basis set used and (ii) the accuracy of the approximated modes used for the computation of the nonlocal electron-phonon coupling. In Fig. 3 we report three scatter plots comparing the results of our calculations of transfer integrals for molecules in Fig. 1 using different functionals and basis sets (B3LYP/3-21g*, B3LYP/6-31g*, B3LYP/6-311g** and PBE/6-31g*). As expected, all of them lead to very similar values.

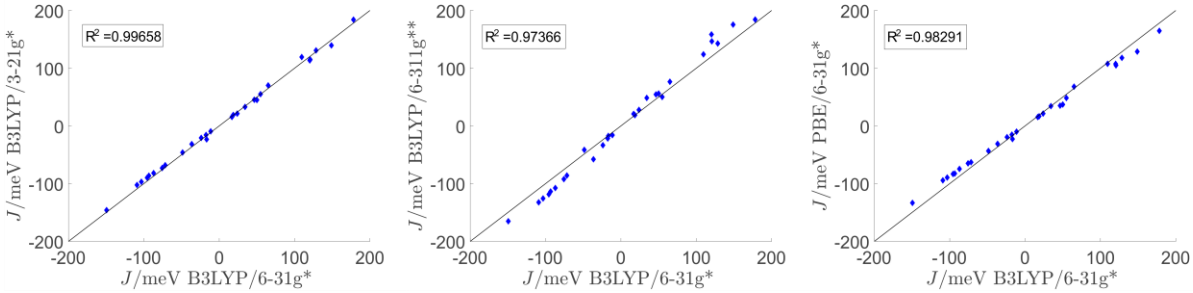

Figure 3. Comparison between transfer integrals for the molecules shown in Fig. 1 obtained with B3LYP/6-31g* vs. B3LYP/3-21g* (left), B3LYP/6-311g** (centre) and PBE/6-31g* (right), respectively.

Moreover, since the transient localization approach only depends on the relative magnitude and sign of the coupling,[21] it is quite insensitive to the (little) variations shown in Fig. 3. With this in mind, we decided to compute the numerical derivatives for the evaluation of the gradient of transfer integral using B3LYP/3-21g*, i.e. the cheapest method, to shorten the computational time, since the evaluation of the gradient of transfer integral is a computationally intensive step, requiring $12\times N_A$ single-point calculations. For consistency with the computations of ∇J, also the J reported in Table 1 are obtained at B3LYP/3-21g* level. Finally we mention that our transfer integral results are in good agreement with data obtained with the latter approach and reported in the literature,[2,13,74] except for rubrene, for which smaller values have been reported using different approximated methodology.[2,74,75]

We next checked the quality of the modes Q obtained with our approximations by defining a spectral density function for the nonlocal electron-phonon coupling:

$$B_{ij}(\omega) = \frac{1}{2\hbar}\sum_M g_{ij,M}^2 \delta(\omega - \omega_M), \tag{12}$$

where the contribution of each mode is weighted by the square of non-local electron-phonon coupling.[76] In the numerical analysis, the Dirac delta function is replaced by a finite broadening (a Gaussian distribution with standard deviation of 5 cm^{-1}). This quantity has been evaluated for two test cases, the couple of Tn and Rb with largest total fluctuations, and our results have been compared with the spectral density computed with a more accurate approach incorporating the effect of phonon band dispersion.[48] As shown in Fig. 4, in light of the strong approximations applied, we have a good agreement between the two approaches, ensuring the reliability of our method. The best figure of merit to compare the two approaches is the room temperature fluctuation of the transfer integral computed as in eq. (5), which gives greater weight to the differences at lower energy. Indeed, as reported in Table 1, the corresponding σ values obtained using the two approaches are very similar, e.g. within 20%, suggesting that using very approximate crystal vibration can be acceptable at least for very rigid molecules. The table also reports values computed by other groups with other methods at a similar level of approximation,[38,43] where the evaluation of the optical phonons was conducted neglecting the

dispersion of the modes with momentum for supercells of different sizes to reach convergence, and the results are reassuringly consistent.

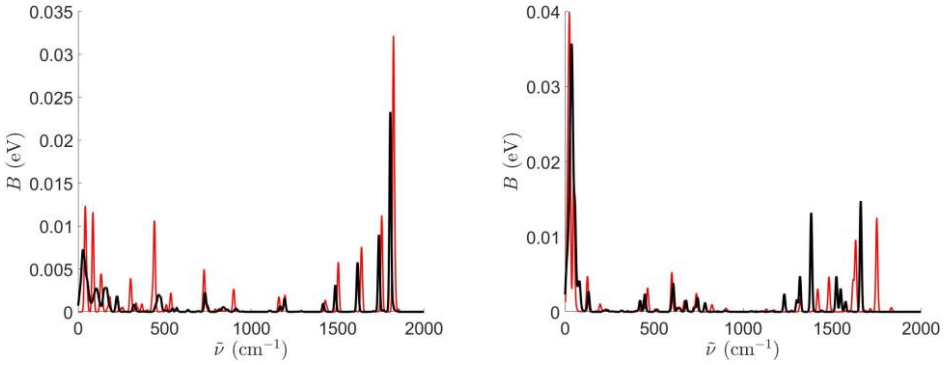

Figure 4. Total spectral density for Tn dimer B (left) and Rb dimer A (right). Black line: our data, red line: data from ref. [48].

Discussion

The main significance of Table 1 and of the validation tests is that it is possible to explore a range of materials to look at the strength of their non-local electron-phonon coupling, i.e. to use our approximate methodology in the area of materials discovery. In particular, the computation of phonons, that represents the slow step in other approaches, requiring up to several months, can be performed using our methodology on a time scale comparable to the evaluation of the gradient of transfer integral, so that the computations of J, ∇J and σ takes about 2-3 days for each system studied (using 16 processors). As could have been anticipated from the methodology itself, our approach can be more inaccurate for molecules containing highly flexible or large fragment like the two alkyl chains in C8-BTBT. Large amplitude vibrations of the isolated molecule are modified by the crystal field (shifted at higher energy and reduced in amplitude) while in the current version of the method this effect is excluded, and the non-local electron phonon coupling is probably overestimated in such molecules.

To the best of our knowledge, this is the first time that the non-local electron-phonon coupling has been evaluated for a quite large set of molecules, and that allows us to identify some general trends and relations among the computed quantities. For example, it is expected that molecules showing high transfer integrals and a low degree of disorder should be the best semiconducting materials and the limited number of reports so far suggested that the relative fluctuation $\sigma/|J|$ falls within a relatively narrow range around 0.5 at room temperature. The analysis of all the data points suggests instead that σ and J are virtually uncorrelated as shown from a scatter plot and a histogram illustrating the distribution of $\sigma/|J|$ in Fig. 5. An immediate consequence of this observation is that there is a potentially large range of $\sigma/|J|$, i.e. the dynamic disorder is not approximately constant – and therefore unavoidable – within the family of molecular semiconductors and one can develop materials where it is substantially smaller. For the same reason, focusing only on materials showing high transfer integrals could be misleading, since a high transfer integral alone does not ensure good semiconducting properties. To give further examples, it is expected that, if $\sigma/|J|$ is very large, the material should display a very poor mobility. Indeed, the molecule displaying the highest values of $\sigma/|J|$ for all the interacting couples, i.e. TIPS (black dashed circles in Fig. 5), has the lowest experimental mobilities reported among the molecules under investigation (0.6 $cm^2V^{-1}s^{-1}$)[21]. On the other hand, a low ratio $\sigma/|J|$ is found for both high mobility materials (e.g. DNTT and Pc, for which have been reported mobilities up to 8.3 $cm^2V^{-1}s^{-1}$ and 9.0 $cm^2V^{-1}s^{-1}$ respectively[77,78]), and for materials with moderate mobility (Pn, with experimental mobility[79–81] of 1.5 $cm^2V^{-1}s^{-1}$). There are at least two reasons for this occurrence: (i) as shown elsewhere[21] the relative sign of the transfer integrals should be also taken into account (it explains the relatively low mobility of Pn) and (ii) experimental data are strongly dependent on the degree of purification of the crystal and therefore one can expect to see the intrinsic mobility for a number of materials that have ideal electronic properties only when extremely pure. We point out that, given the large spread of values that can be found in the literature, in particular for pentacene, we have considered only experimental mobility results showing good reproducibility between different groups, as these are as close to the ideal intrinsic behaviour as can be achieved today.[21]

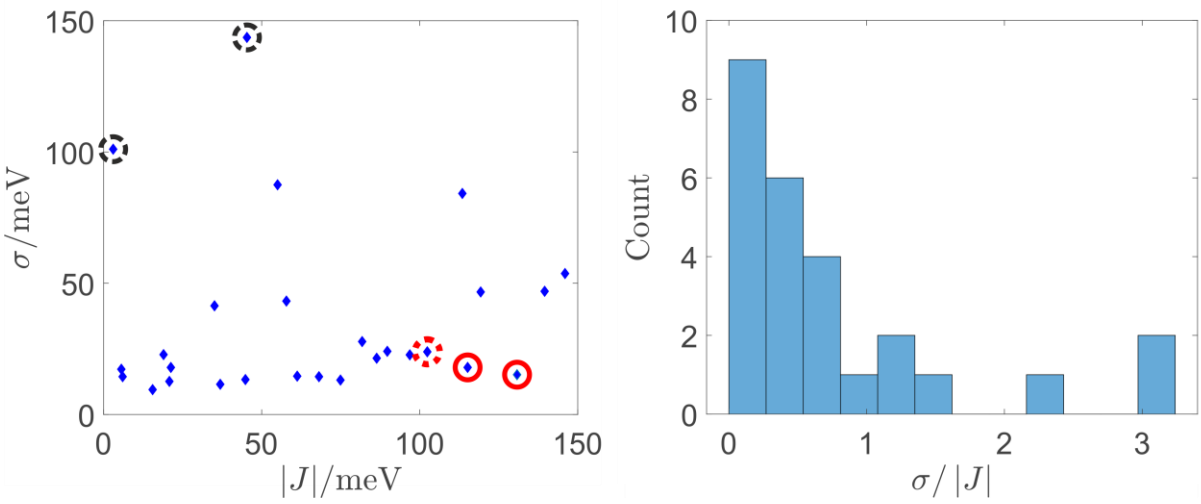

Figure 5. Scatter plot showing σ vs. absolute value of J (left) and histogram of $\sigma/|J|$ (right) for all the couples reported in Table 1. Black dashed circles identify TIPS values, red dotted circles identify Pn-B and red full circles identify DNTT-A and Pc-A values. The rather high $\sigma/|J|$ for TIPS is not reported in the histogram for convenience.

The data in Table 1 can also be used to establish whether the main contributor to the disorder σ is the strength of the transfer integral gradient (∇J) or the polarization of the phonons (Q_M). There is, broadly speaking, a good correlation between σ and $|\nabla J|$, as illustrated in Fig. 6, suggesting that ∇J is the main factor determining the strength of the fluctuation of the transfer integral. In particular, as it is also clear from the definition of σ (eq. (5) and (9)), smaller $|\nabla J|$ are always associated with small disorder while, for larger $|\nabla J|$, there is a larger distribution of values for σ, which is affected by the phonon polarization direction. Fig. 6 highlights the case of TIPS and BTBT, which have similar $|\nabla J|$ values and very different σ. The implication for materials discovery is that one should focus on the identification of materials with small $|\nabla J|$, a property that can be computed more easily and does not depend on vibrational properties of the solids.

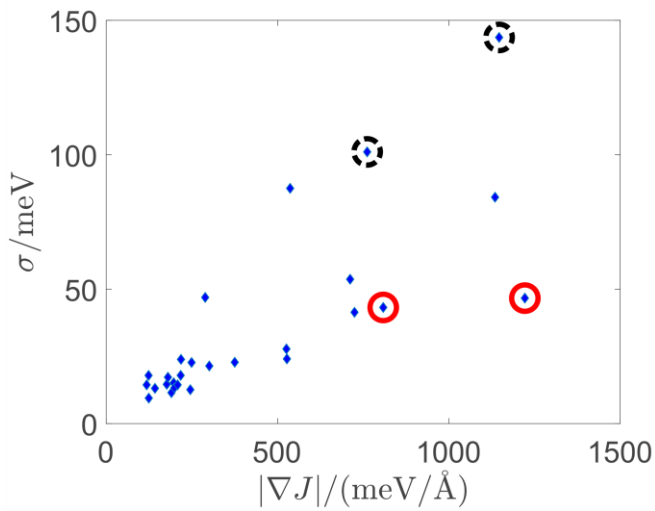

Figure 6. Scatter plot showing σ vs. $|\nabla J|$ for all the couples reported in Table 1. Black dashed circles highlight TIPS values, while red circles identify BTBT values.

To explain more intuitively the role of phonon polarization, e.g. how materials with similar $|\nabla J|$ may have very different σ, we resort to a graphical representation of eq. (9), that expresses the electron-phonon coupling as the scalar product between the gradient of transfer integral and the phonon displacements (Q_M). In Fig. 7 we graphically represent these two quantities as a set of red (∇J) and green (Q_M) arrows centred on the corresponding atom for the mode showing the highest contributions to total σ for BTBT-A (ω=58 cm^{-1}) and TIPS-C (ω=15 cm^{-1}). It is easy to notice that, in the case of BTBT, the mode displacements are almost orthogonal to the gradient of transfer integral, thus leading to a low value of σ despite the quite high value of

$|\nabla J|$ (see Table 1). On the contrary, for TIPS, the couple showing the highest value of σ, the gradient of transfer integral shows a good overlap with the phonon displacements. While the role of the phonon polarization in determining the fluctuation of the transfer integral can be therefore fully explained, it is very difficult to design molecular materials with the desired phonon characteristics also because of the high computational cost of these calculations.

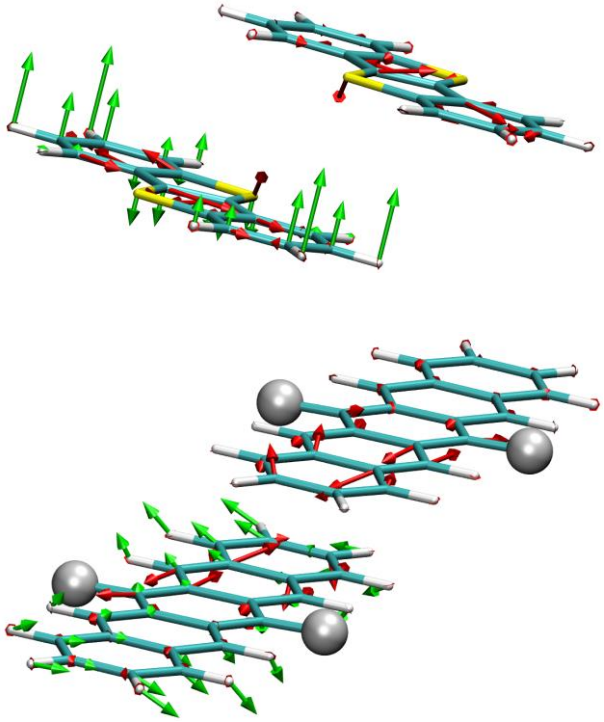

Figure 7. Superposition of the gradient of the transfer integral (red arrows) and the displacements (green arrows) for the mode showing the greatest contribution to the total σ for: top BTBT; bottom TIPS (the Si atoms and the alkyl chains, which have almost zero values of ∇J, are replaced by a grey sphere). Note that the displacements are shown only on one molecule since in our approach the crystal vibrations are localized on one molecule.

The analysis so far suggests that, to design better molecular semiconductors, one should develop an intuitive understanding of what makes the transfer integral less sensitive to the nuclear motion or, more quantitatively, what makes the ratio $|\nabla J|/|J|$ as small as possible. In the early papers of organic electronics,[82] researchers focus on the intermolecular geometries that maximize the transfer integrals. In a similar way we can construct a joint map of $|\nabla J|$ and $|J|$ ratio to understand how and why some mutual molecular configuration are less susceptible to dynamic disorder.

To provide an initial illustration of this point, we have evaluated $|\nabla J|$ and $|J|$ for different relative positions of two molecules in the DNTT-A couple, which displays a rather low $|\nabla J|/|J|$ value. In particular, starting from the crystallographic mutual geometry we translate one molecule with respect to the other along the short molecular axis Δx as shown in Fig. 8 ($\Delta x=\Delta y=\Delta z=0$ is the equilibrium geometry). $|\nabla J|$ and $|J|$ seems to follow independent behaviours, e.g. there is no relation between the maxima of $|J|$ and the value of $|\nabla J|$. For this reason, in the interval 1 Å$<\Delta x<$7 Å, where the molecules have good overlap, one obviously observes a small ratio $|\nabla J|/|J|$ when $|J|$ is large, i.e. 4.5 Å$<\Delta x<$ 5.6 Å. A less trivial area interesting for good transport properties is when the overlap between the two molecules is limited to only few atoms, e.g. in the region ($\Delta x<0$ Å). Also in this case the ratio $|\nabla J|/|J|$ becomes small, this time because $|\nabla J|$ is smaller when fewer atoms are involved in the transfer integral (the displacement of the atoms not involved does not influence the transfer integral).

This analysis suggests that molecular crystals where molecules interact through their extremities should not be dismissed as this arrangement can be highly beneficial for small non-local electron-phonon couplings. Such observation may explain for example the difference between DTTTF-A and DNTT-A, two systems possessing

similar J values but significantly different $|\nabla J|$ (see Table 1). Indeed, as shown in Fig. 9, where the HOMO orbitals of these two systems are shown, it is easy to notice that the two DTTTF molecules show a partial stacking, while the DNTT molecules interact through their extremities.

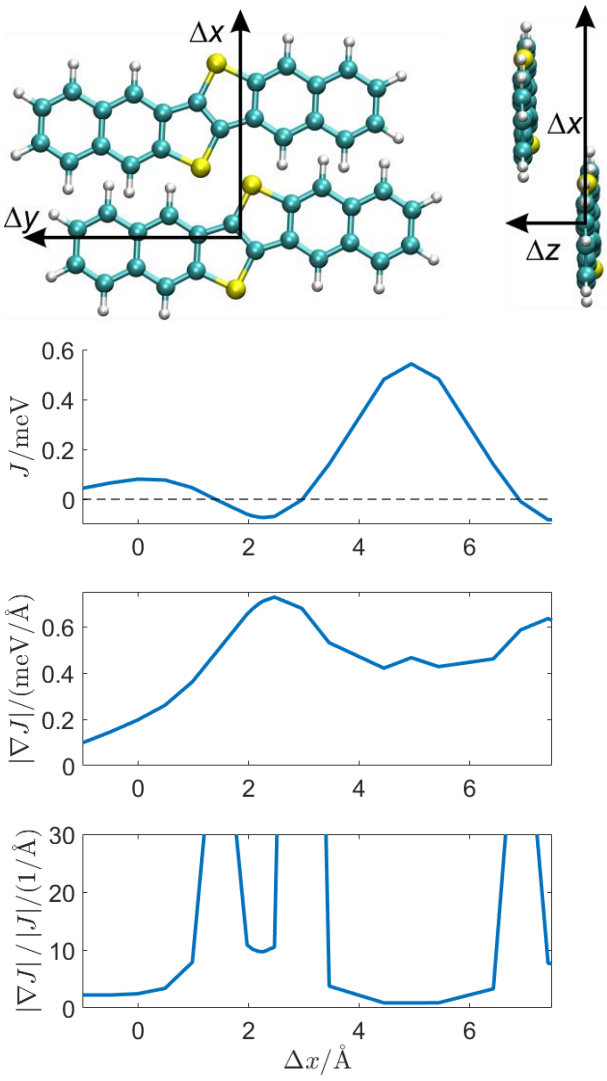

Figure 8. Top: reference frame for the relative shift of the two DNTT molecules. Below, a plot showing: values of J (top), $|\nabla J|$ (middle) and $|\nabla J|/J$ (bottom) for different relative positions of the two molecules in the DNTT-A couple. As shown on the top reference frame, positive Δx values mean that the molecules are rigidly shifted towards the direction in which they are closer than experimental geometry.

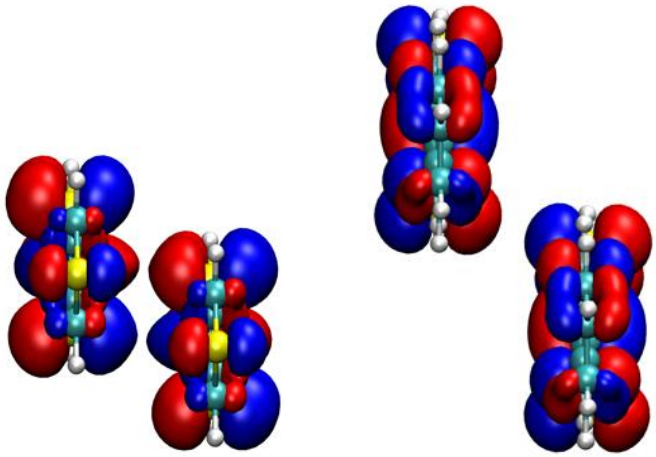

Figure 9. Side view of DTTF-A (left) and DNTT-A (right) HOMO orbitals.

Conclusions

In conclusion, in this paper we have presented a methodology for the quick evaluation of the non-local electron-phonon coupling relying on two main approximations: the evaluation of the Cartesian gradient of transfer integral and the use of approximated phonons evaluated within the rigid body approximation. Despite the severe approximations, our method leads to results in excellent agreement with data obtained with more accurate approaches.

The good number of molecules studied by this approach allows us to outline some general trends. First of all, we have shown that there is almost no correlation between the transfer integral J and their room temperature fluctuation σ. For this reason, the fluctuation of the transfer integral should not be considered an unavoidable property of these materials and, on the contrary, one could search for materials for which the ratio σ/J is minimized. Secondly, since our data point out that materials with small σ are invariably characterized by small values of the gradient of the transfer integral with respect to all atomic translations $|\nabla J|$, and this quantity is substantially cheaper to evaluate, we highlight the possibility of using $|\nabla J|$ instead of σ to identify materials showing low dynamic disorder. Following these ideas, we propose that the best mutual arrangement between molecules can be deduced by comparing the map of the transfer integral (well known since the early days of organic electronics) with the map of its gradient (proposed here). Using the test case of the DNTT molecule we showed that favourable regions for transport can be found near the maxima of J (as expected) but also when the molecules interact through their edges which form a minimum for $|\nabla J|$.

In summary, this work provides an efficient way to access an important quantity for charge transport in molecular crystals. Its computation on larger molecular databases and on new molecules is expected to guide the rationalization of the charge transport characteristics of this class of materials.

Acknowledgements

The authors are grateful to Xiaoyu Xie and Alejandro Santana-Bonilla for helpful suggestions. A. L. gratefully acknowledges the support of the Erasmus+ programme. A. T. acknowledges financial support from ERC (Grant No. 615834) and EPSRC.

References

(1) Wang, C.; Dong, H.; Jiang, L.; Hu, W. Organic Semiconductor Crystals. *Chem. Soc. Rev.* **2018**, *47*,

422–500.

(2) Coropceanu, V.; Cornil, J.; da Silva Filho, D. A.; Olivier, Y.; Silbey, R.; Brédas, J.-L. Charge Transport in Organic Semiconductors. *Chem. Rev.* **2007**, *107*, 926–952.

(3) Mei, J.; Diao, Y.; Appleton, A. L.; Fang, L.; Bao, Z. Integrated Materials Design of Organic Semiconductors for Field-Effect Transistors. *J. Am. Chem. Soc.* **2013**, *135*, 6724–6746.

(4) Facchetti, A. Semiconductors for Organic Transistors. *Mater. Today* **2007**, *10*, 28–37.

(5) Brütting, W.; Frischeisen, J.; Schmidt, T. D.; Scholz, B. J.; Mayr, C. Device Efficiency of Organic Light-Emitting Diodes: Progress by Improved Light Outcoupling. *Phys. Status Solidi Appl. Mater. Sci.* **2013**, *210*, 44–65.

(6) Kippelen, B.; Bredas, J.-L. Organic Photovoltaics. *Energy Environ. Sci.* **2009**, *2*, 251–261.

(7) Dong, H.; Wang, C.; Hu, W. High Performance Organic Semiconductors for Field-Effect Transistors. *Chem. Commun.* **2010**, *46*, 5211–5222.

(8) Akimov, A. V.; Prezhdo, O. V. Large-Scale Computations in Chemistry: A Bird's Eye View of a Vibrant Field. *Chem. Rev.* **2015**, *115*, 5797–5890.

(9) Hachmann, J.; Olivares-Amaya, R.; Atahan-Evrenk, S.; Amador-Bedolla, C.; Sánchez-Carrera, R. S.; Gold-Parker, A.; Vogt, L.; Brockway, A. M.; Aspuru-Guzik, A. The Harvard Clean Energy Project: Large-Scale Computational Screening and Design of Organic Photovoltaics on the World Community Grid. *J. Phys. Chem. Lett.* **2011**, *2*, 2241–2251.

(10) Liu, Y.; Zhao, T.; Ju, W.; Shi, S.; Shi, S.; Shi, S. Materials Discovery and Design Using Machine Learning. *J. Mater.* **2017**, *3*, 159–177.

(11) Price, S. L. Predicting Crystal Structures of Organic Compounds. *Chem. Soc. Rev.* **2014**, *43*, 2098–2111.

(12) Needs, R. J.; Pickard, C. J. Perspective: Role of Structure Prediction in Materials Discovery and Design. *APL Mater.* **2016**, *4*, 053210.

(13) Yavuz, I.; Martin, B. N.; Park, J.; Houk, K. N. Theoretical Study of the Molecular Ordering, Paracrystallinity, and Charge Mobilities of Oligomers in Different Crystalline Phases. *J. Am. Chem. Soc.* **2015**, *137*, 2856–2866.

(14) Landi, A.; Borrelli, R.; Capobianco, A.; Velardo, A.; Peluso, A. Hole Hopping Rates in Organic Semiconductors: A Second-Order Cumulant Approach. *J. Chem. Theory Comput.* **2018**, *14*, 1594–1601.

(15) Nguyen, T. P.; Shim, J. H.; Lee, J. Y. Density Functional Theory Studies of Hole Mobility in Picene and Pentacene Crystals. *J. Phys. Chem. C* **2015**, *119*, 11301–11310.

(16) Schober, C.; Reuter, K.; Oberhofer, H. Virtual Screening for High Carrier Mobility in Organic Semiconductors. *J. Phys. Chem. Lett.* **2016**, *7*, 3973–3977.

(17) Troisi, A. The Speed Limit for Sequential Charge Hopping in Molecular Materials. *Org. Electron. physics, Mater. Appl.* **2011**, *12*, 1988–1991.

(18) Okada, Y.; Sakai, K.; Uemura, T.; Nakazawa, Y.; Takeya, J. Charge Transport and Hall Effect in Rubrene Single-Crystal Transistors under High Pressure. *Phys. Rev. B* **2011**, *84*, 245308.

(19) Lin, Y. J.; Tsao, H. Y.; Liu, D. S. Hall-Effect Mobility of Pentacene Films Prepared by the Thermal Evaporating Method with Different Substrate Temperature. *Appl. Phys. Lett.* **2012**, *101*, 013302.

(20) Troisi, A.; Orlandi, G. Charge-Transport Regime of Crystalline Organic Semiconductors: Diffusion Limited by Thermal off-Diagonal Electronic Disorder. *Phys. Rev. Lett.* **2006**, *96*, 086601.

(21) Fratini, S.; Ciuchi, S.; Mayou, D.; De Laissardière, G. T.; Troisi, A. A Map of High-Mobility Molecular Semiconductors. *Nat. Mater.* **2017**, *16*, 998–1002.

(22) Ortmann, F.; Bechstedt, F.; Hannewald, K. Charge Transport in Organic Crystals: Theory and Modelling. *Phys. Status Solidi* **2011**, *248*, 511–525.

(23) Illig, S.; Eggeman, A. S.; Troisi, A.; Jiang, L.; Warwick, C.; Nikolka, M.; Schweicher, G.; Yeates, S. G.; Henri Geerts, Y.; Anthony, J. E.; et al. Reducing Dynamic Disorder in Small-Molecule Organic Semiconductors by Suppressing Large-Amplitude Thermal Motions. *Nat. Commun.* **2016**, *7*, 10736.

(24) Troisi, A. Dynamic Disorder in Molecular Semiconductors: Charge Transport in Two Dimensions. *J. Chem. Phys.* **2011**, *134*, 034702.

(25) Wang, L.; Beljonne, D. Flexible Surface Hopping Approach to Model the Crossover from Hopping to Band-like Transport in Organic Crystals. *J. Phys. Chem. Lett.* **2013**, *4*, 1888–1894.

(26) Giannini, S.; Carof, A.; Blumberger, J. Crossover from Hopping to Band-Like Charge Transport in an Organic Semiconductor Model: Atomistic Non-Adiabatic Molecular Dynamics Simulation. *J. Phys. Chem. Lett.* **2018**, *9*, 3116–3123.

(27) Lee, C. K.; Moix, J.; Cao, J. Coherent Quantum Transport in Disordered Systems: A Unified Polaron Treatment of Hopping and Band-like Transport. *J. Chem. Phys.* **2015**, *142*, 164103.

(28) Packwood, D. M.; Oniwa, K.; Jin, T.; Asao, N. Charge Transport in Organic Crystals: Critical Role of Correlated Fluctuations Unveiled by Analysis of Feynman Diagrams. *J. Chem. Phys.* **2015**, *142*, 144503.

(29) De Filippis, G.; Cataudella, V.; Mishchenko, A. S.; Nagaosa, N.; Fierro, A.; De Candia, A. Crossover from Super- to Subdiffusive Motion and Memory Effects in Crystalline Organic Semiconductors. *Phys. Rev. Lett.* **2015**, *114*, 086601.

(30) Chen, D.; Ye, J.; Zhang, H.; Zhao, Y. On the Munn−Silbey Approach to Polaron Transport with Off-Diagonal Coupling and Temperature-Dependent Canonical Transformations. *J. Phys. Chem. B* **2011**, *115*, 5312–5321.

(31) Heck, A.; Kranz, J. J.; Kubař, T.; Elstner, M. Multi-Scale Approach to Non-Adiabatic Charge Transport in High-Mobility Organic Semiconductors. *J. Chem. Theory Comput.* **2015**, *11*, 5068–5082.

(32) Borrelli, R.; Capobianco, A.; Landi, A.; Peluso, A. Vibronic Couplings and Coherent Electron Transfer in Bridged Systems. *Phys. Chem. Chem. Phys.* **2015**, *4*, 1166–1169.

(33) Heck, A.; Kranz, J. J.; Elstner, M. Simulation of Temperature-Dependent Charge Transport in Organic Semiconductors with Various Degrees of Disorder. *J. Chem. Theory Comput.* **2016**, *12*, 3087–3096.

(34) Spencer, J.; Gajdos, F.; Blumberger, J. FOB-SH: Fragment Orbital-Based Surface Hopping for Charge Carrier Transport in Organic and Biological Molecules and Materials. *J. Chem. Phys.* **2016**, *145*, 064102.

(35) Ishii, H.; Honma, K.; Kobayashi, N.; Hirose, K. Wave-Packet Approach to Transport Properties of Carrier Coupled with Intermolecular and Intramolecular Vibrations of Organic Semiconductors. *Phys. Rev. B* **2012**, *85*, 245206.

(36) Ciuchi, S.; Fratini, S. Electronic Transport and Quantum Localization Effects in Organic Semiconductors. *Phys. Rev. B* **2012**, *86*, 245201.

(37) Fratini, S.; Mayou, D.; Ciuchi, S. The Transient Localization Scenario for Charge Transport in Crystalline Organic Materials. *Adv. Funct. Mater.* **2016**, *26*, 2292–2315.

(38) Sánchez-Carrera, R. S.; Paramonov, P.; Day, G. M.; Coropceanu, V.; Brédas, J. L. Interaction of Charge Carriers with Lattice Vibrations in Oligoacene Crystals from Naphthalene to Pentacene. *J. Am. Chem. Soc.* **2010**, *132*, 14437–14446.

(39) Ordejón, P.; Boskovic, D.; Panhans, M.; Ortmann, F. Ab Initio Study of Electron-Phonon Coupling in Rubrene. *Phys. Rev. B* **2017**, *96*, 035202.

(40) Nyman, J.; Pundyke, O. S.; Day, G. M. Accurate Force Fields and Methods for Modelling Organic Molecular Crystals at Finite Temperatures. *Phys. Chem. Chem. Phys.* **2016**, *18*, 15828–15837.

(41) Howard, J. A. K.; Allen, F. H.; Shields, G. P. *Implications of Molecular and Materials Structure for New Technologies*; Springer, Berlin 2012.

(42) Kim, J.; Kwon, O. P.; Brunner, F. D. J.; Jazbinsek, M.; Lee, S. H.; Günter, P. Phonon Modes of Organic Electro-Optic Molecular Crystals for Terahertz Photonics. *J. Phys. Chem. C* **2015**, *119*, 10031–10039.

(43) Yi, Y.; Coropceanu, V.; Brédas, J. L. Nonlocal Electron-Phonon Coupling in the Pentacene Crystal: Beyond the Γ-Point Approximation. *J. Chem. Phys.* **2012**, *137*, 164303.

(44) Venuti, E.; Della Valle, R. G.; Farina, L.; Brillante, A.; Masino, M.; Girlando, A. Phonons and Structures of Tetracene Polymorphs at Low Temperature and High Pressure. *Phys. Rev. B* **2004**, *70*, 104106.

(45) Abdulla, M.; Refson, K.; Friend, R. H.; Haynes, P. D. A First-Principles Study of the Vibrational Properties of Crystalline Tetracene under Pressure. *J. Phys. Condens. Matter* **2015**, *27*, 375402.

(46) Coropceanu, V.; Sanchez-Carrera, R. S.; Paramonov, P.; Day, G. M.; Brédas, J. Interaction of Charge Carriers with Lattice Vibrations in Organic Molecular Semiconductors : Naphthalene as a Case Study Interaction of Charge Carriers with Lattice Vibrations in Organic Molecular Semiconductors : Naphthalene as a Case Study. *J. Phys. Chem. C* **2009**, *113*, 4679–4686.

(47) Lee, N. E.; Zhou, J. J.; Agapito, L. A.; Bernardi, M. Charge Transport in Organic Molecular Semiconductors from First Principles: The Bandlike Hole Mobility in a Naphthalene Crystal. *Phys. Rev. B* **2018**, *97*, 115203.

(48) Xie, X.; Santana-Bonilla, A.; Troisi, A. Nonlocal Electron-Phonon Coupling in Prototypical Molecular Semiconductors from First Principles. *J. Chem. Theory Comput.* **2018**, acs.jctc.8b00235.

(49) Troisi, A.; Orlandi, G. The Hole Transfer in DNA: Calculation of Electron Coupling between Close Bases. *Chem. Phys. Lett.* **2001**, *344*, 509–518.

(50) Xie, Y.; Zheng, J.; Lan, Z. Full-Dimensional Multilayer Multiconfigurational Time-Dependent Hartree Study of Electron Transfer Dynamics in the Anthracene/C60 Complex. *J. Chem. Phys.* **2015**, *142*, 084706.

(51) Venuti, E.; Bilotti, I.; Della Valle, R. G.; Brillante, A.; Ranzieri, P.; Masino, M.; Girlando, A. Polarized Raman Spectra of a Rubrene Single Crystal. *J. Phys. Chem. C* **2008**, *112*, 17416–17422.

(52) Schettino, V. Infrared and Raman Spectra of Crystalline Triphenylene and Triphenylene-D12 and Normal Coordinates Calculations. *J. Mol. Spectrosc.* **1970**, *34*, 78–96.

(53) Girlando, A.; Grisanti, L.; Masino, M.; Bilotti, I.; Brillante, A.; Della Valle, R. G.; Venuti, E. Peierls and Holstein Carrier-Phonon Coupling in Crystalline Rubrene. *Phys. Rev. B* **2010**, *82*, 035208.

(54) Li, Y.; Coropceanu, V.; Brédas, J. L. Nonlocal Electron-Phonon Coupling in Organic Semiconductor Crystals: The Role of Acoustic Lattice Vibrations. *J. Chem. Phys.* **2013**, *138*, 204713.

(55) Hannewald, K.; Stojanović, V. M.; Schellekens, J. M. T.; Bobbert, P. A.; Kresse, G.; Hafner, J. Theory of Polaron Bandwidth Narrowing in Organic Molecular Crystals. *Phys. Rev. B* **2004**, *69*, 075211.

(56) Aradi, B.; Hourahine, B.; Frauenheim, T. DFTB+, a Sparse Matrix-Based Implementation of the DFTB Method. *J. Phys. Chem. A* **2007**, *111*, 5678–5684.

(57) Elstner, M.; Porezag, D.; Jungnickel, G.; Elsner, J.; Haugk, M.; Frauenheim, T.; Suhai, S.; Seifert, G. Self-Consistent-Charge Density-Functional Tight-Binding Method for Simulations of Complex Materials Properties. *Phys. Rev. B* **1998**, *58*, 7260–7268.

(58) Seifert, G.; Joswig, J. O. Density-Functional Tight Binding-an Approximate Density-Functional Theory Method. *Wiley Interdiscip. Rev. Comput. Mol. Sci.* **2012**, *2*, 456–465.

(59) Monkhorst, H. J.; Pack, J. D. Special Points for Brillouin-Zone Integrations. *Phys. Rev. B* **1976**, *13*, 5188–5192.

(60) Grimme, S.; Antony, J.; Ehrlich, S.; Krieg, H. A Consistent and Accurate Ab Initio Parametrization of Density Functional Dispersion Correction (DFT-D) for the 94 Elements H-Pu. *J. Chem. Phys.* **2010**, *132*, 154104.

(61) Frisch, M. J.; Trucks, G. W.; Schlegel, H. B.; Scuseria, G. E.; Robb, M. A.; Cheeseman, J. R.; Scalmani, G.; Barone, V.; Petersson, G. A.; Nakatsuji, H.; et al. Gaussian 16, Revision A.03. Gaussian, Inc: Wallingford CT 2016.

(62) Kubas, A.; Gajdos, F.; Heck, A.; Oberhofer, H.; Elstner, M.; Blumberger, J. Electronic Couplings for Molecular Charge Transfer: Benchmarking CDFT, FODFT and FODFTB against High-Level Ab Initio Calculations. II. *Phys. Chem. Chem. Phys.* **2015**, *17*, 14342–14354.

(63) Kubas, A.; Hoffmann, F.; Heck, A.; Oberhofer, H.; Elstner, M.; Blumberger, J. Electronic Couplings for Molecular Charge Transfer: Benchmarking CDFT, FODFT, and FODFTB against High-Level Ab Initio Calculations. *Phys. Chem. Chem. Phys.* **2014**, *140*, 14342–14354.

(64) Kubar, T.; Woiczikowski, P. B.; Cuniberti, G.; Elstner, M. Efficient Calculation of Charge-Transfer Matrix Elements for Hole Transfer in DNA. *J. Phys. Chem. B* **2008**, *112*, 7937–7947.

(65) Oliveira, A. F.; Seifert, G.; Heine, T.; Duarte, H. A. Density-Functional Based Tight-Binding: An Approximate DFT Method. *J. Braz. Chem. Soc.* **2009**, *20*, 1193–1205.

(66) Li, W.; Kotsis, K.; Manzhos, S. Comparative Density Functional Theory and Density Functional Tight Binding Study of Arginine and Arginine-Rich Cell Penetrating Peptide TAT Adsorption on Anatase TiO2. *Phys. Chem. Chem. Phys.* **2016**, *18*, 19902–19917.

(67) Wang, C.; Dong, H.; Hu, W.; Liu, Y.; Zhu, D. Semiconducting π-Conjugated Systems in Field-Effect Transistors: A Material Odyssey of Organic Electronics. *Chem. Rev.* **2012**, *112*, 2208–2267.

(68) Deng, W. Q.; Sun, L.; Huang, J. D.; Chai, S.; Wen, S. H.; Han, K. L. Quantitative Prediction of Charge Mobilities of π-Stacked Systems by First-Principles Simulation. *Nat. Protoc.* **2015**, *10*, 632–642.

(69) Shuai, Z.; Wang, L.; Chenchen, S. *Theory of Charge Transport in Carbon Electronic Materials*; Springer, Berlin, 2012.

(70) Sundar, V. C.; Zaumseil, J.; Podzorov, V.; Menard, E.; Willett, R. L.; Someya, T.; Gershenson, M. E.; Rogers, J. a. Elastomeric Transistor Stamps : Transport in Organic Crystals. *Science* **2004**, *303*, 1644–1646.

(71) Blülle, B.; Troisi, A.; Häusermann, R.; Batlogg, B. Charge Transport Perpendicular to the High Mobility Plane in Organic Crystals: Bandlike Temperature Dependence Maintained despite Hundredfold Anisotropy. *Phys. Rev. B* **2016**, *93*, 035205.

(72) Groom, C. R.; Bruno, I. J.; Lightfoot, M. P.; Ward, S. C. The Cambridge Structural Database. *Acta Crystallogr. Sect. B Struct. Sci. Cryst. Eng. Mater.* **2016**, *72*, 171–179.

(73) Troisi, A. Prediction of the Absolute Charge Mobility of Molecular Semiconductors: The Case of Rubrene. *Adv. Mater.* **2007**, *19*, 2000–2004.

(74) Kobayashi, H.; Kobayashi, N.; Hosoi, S.; Koshitani, N.; Murakami, D.; Shirasawa, R.; Kudo, Y.; Hobara, D.; Tokita, Y.; Itabashi, M. Hopping and Band Mobilities of Pentacene, Rubrene, and 2,7-Dioctyl[1] Benzothieno[3,2-b][1]Benzothiophene (C8-BTBT) from First Principle Calculations. *J. Chem. Phys.* **2013**, *139*, 014707.

(75) Baumeier, B.; Kirkpatrick, J.; Andrienko, D. Density-Functional Based Determination of Intermolecular Charge Transfer Properties for Large-Scale Morphologies. *Phys. Chem. Chem. Phys.* **2010**, *12*, 11103–11113.

(76) Aghtar, M.; Liebers, J.; Strümpfer, J.; Schulten, K.; Kleinekathöfer, U. Juxtaposing Density Matrix and Classical Path-Based Wave Packet Dynamics. *J. Chem. Phys.* **2012**, *136*, 214101.

(77) Haas, S.; Takahashi, Y.; Takimiya, K.; Hasegawa, T. High-Performance Dinaphtho-Thieno-Thiophene Single Crystal Field-Effect Transistors. *Appl. Phys. Lett.* **2009**, *95*, 2007–2010.

(78) Xin, Q.; Duhm, S.; Bussolotti, F.; Akaike, K.; Kubozono, Y.; Aoki, H.; Kosugi, T.; Kera, S.; Ueno, N. Accessing Surface Brillouin Zone and Band Structure of Picene Single Crystals. *Phys. Rev. Lett.* **2012**, *108*, 226401.

(79) Lee, J. Y.; Roth, S.; Park, Y. W. Anisotropic Field Effect Mobility in Single Crystal Pentacene. *Appl. Phys. Lett.* **2006**, *88*, 252106.

(80) Uemura, T.; Yamagishi, M.; Soeda, J.; Takatsuki, Y.; Okada, Y.; Nakazawa, Y.; Takeya, J. Temperature Dependence of the Hall Effect in Pentacene Field-Effect Transistors: Possibility of Charge Decoherence Induced by Molecular Fluctuations. *Phys. Rev. B* **2012**, *85*, 035313.

(81) Takeyama, Y.; Ono, S.; Matsumoto, Y. Organic Single Crystal Transistor Characteristics of Single-Crystal Phase Pentacene Grown by Ionic Liquid-Assisted Vacuum Deposition. *Appl. Phys. Lett.* **2012**, *101*, 083303.

(82) Brédas, J. L.; Calbert, J. P.; da Silva Filho, D. A.; Cornil, J. Organic Semiconductors: A Theoretical Characterization of the Basic Parameters Governing Charge Transport. *Proc. Natl. Acad. Sci. USA* **2002**, *99*, 5804–5809.

TOC graphic